J Clust Sci (2010) 21:485–501
DOI 10.1007/s10876-010-0324-8

ORIGINAL PAPER

A Family of 3-D Coordination Polymers Composed of Mixed-Valence Mn_6 Octahedra within Na_4 Tetrahedra

Theocharis C. Stamatatos · Khalil A. Abboud · George Christou

Received: 23 March 2010 / Published online: 25 May 2010

Abstract The combined use of 1,1,1-tris(hydroxymethyl)ethane ($thmeH_3$) and azides in Mn carboxylate chemistry has yielded a new family of decanuclear $[Mn_6Na_4O(N_3)(O_2CR)_5(thme)_4(H_2O)_4]$ (R = Me (**1**); Et (**2**)) complexes consisting of mixed-valence $Mn^{II}_2Mn^{III}_4$ units with a very rare $[Mn_6(\mu_6\text{-}O)]^{14+}$ octahedral core contained within a tetrahedron of four Na^I atoms. The $[Mn_6Na_4]$ units of **1** and **2** are connected via the Na atoms to neighboring units, giving 3-D supramolecular assemblies with large channel cavities. Variable-temperature, solid-state dc and ac magnetization studies carried out in the 1.8–300 K range reveal that the Mn_6 units of **1** and **2** are antiferromagnetically coupled to give $S = 0$ ground states for both complexes.

Keywords Coordination polymers · Magnetochemistry · Mixed-valence manganese clusters · Octahedral topology · 1,1,1-Tris(hydroxymethyl)ethane

Introduction

Molecular polynuclear complexes (clusters) and coordination polymers of paramagnetic 3d metals at intermediate oxidation states continue to be major research areas because of their complex structures and often fascinating physical properties [1]. Manganese cluster chemistry is a central player in the fields of bioinorganic chemistry and molecular magnetism, and has been receiving special attention for

Dedicated to Professor Malcolm H. Chisholm on the occasion of his 65th birthday; an outstanding scientist, colleague, and friend.

T. C. Stamatatos · K. A. Abboud · G. Christou (✉)
Department of Chemistry, University of Florida, Gainesville, FL 32611-7200, USA
e-mail: christou@chem.ufl.edu

two main reasons: (i) the occurrence of this metal in a variety of redox enzymes [2], the most important of which is the {$CaMn_4$} water oxidizing complex (WOC) within the photosynthetic apparatus of green plants and cyanobacteria [3, 4]. As a result, the structures and properties of various synthetic models of the WOC are under active investigation [5–7]; and (ii) high nuclearity Mn complexes often display large ground state spin (*S*) values [8–12] as a result of ferromagnetic exchange interactions and/or spin frustration effects [13, 14]. If such molecules with large *S* values also possess significant magnetoanisotropy of the Ising (easy-axis) type, then they have the potential to be single-molecule magnets (SMMs) [15–20]. These are individual molecules that possess a significant barrier (vs. *kT*) to magnetization relaxation and thus exhibit the ability to function as nanoscale magnets below their blocking temperature (T_B), representing a molecular, 'bottom-up' approach to nanomagnetism [21].

Our group has had a strong interest over many years in the development of synthetic methods to manganese carboxylate [21, 22] and non-carboxylate clusters [12, 23]. We have explored and successfully developed many new routes for the synthesis of Mn cluster complexes with nuclearities up to 84 [24]. As part of this work, we have explored a wide variety of organic groups that can simultaneously be both chelating and bridging ligands, including the anions of 2-(hydroxymethyl)pyridine (hmpH) and related ligands [25–29], 2,6-pyridinedimethanol ($pdmH_2$) [12, 27, 30–32], triethanolamine ($teaH_3$) [33, 34], *N*-methyldiethanolamine ($mdaH_2$) [34–36], and the *gem*-diol form of di-2-pyridylketone ($dpkdH_2$) [37–39], which have proven to foster formation of high nuclearity products (Scheme 1). All these anions are alkoxide-based ligands (with or without pyridyl groups), and their alkoxide arm(s) often support ferromagnetic coupling between the metal ions that they bridge [12, 25, 26, 28–30, 34, 36].

More recently, we started an investigation of the affinity of the azide (N_3^-) ion as an ancillary bridging ligand in higher oxidation state Mn cluster chemistry with

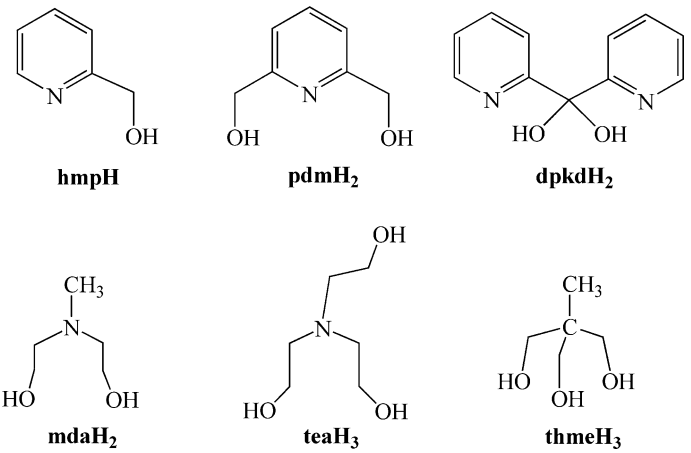

Scheme 1 The protonated precursors to the chelating ligands discussed in the text

chelates such as those above [23]. From a magnetic viewpoint, the N_3^- ion bridging in the 1,1-fashion (end-on) is one of the strongest ferromagnetic mediators in molecular magnetism for a wide range of M–N–M angles [23, 40, 41], and thus it has opened up an attractive alternative route to new high-spin Mn clusters and SMMs. In past work, for example, we have shown that azide and the bidentate (N,O) chelate hmp^- or the tridentate (N,O,O) chelate $pdmH^-/pdm^{2-}$ yield $[Mn_{10}O_4(N_3)_4(hmp)_{12}]^{2+}$ with $S = 22$ [25], and $[Mn_{25}O_{18}(OH)_2(N_3)_{12}(pdm)_6(pdmH)_6]^{2+}$ with $S = {}^{51}/_2$ [30], respectively. Further, when azides were combined with carboxylates and the tetradentate (N,N,O,O) chelate $dpkd^{2-}$, the $[Mn_{26}O_8(OH)_4(N_3)_{12}(O_2CMe)_6(dpkd)_{14}(DMF)_4]$ and $[Mn_{24}O_{10}(N_3)_8(O_2CCMe_3)_{16}(dpkd)_{12}(DMF)_4]$ complexes were obtained, both possessing a covalently-linked dimer-of-clusters structure [38]. All these azide-containing products are high-spin molecules, and the majority of them are SMMs with aesthetically pleasing structures.

In the present work, we have explored reactions under basic conditions of Mn salts with a combination of azide, carboxylate, and the potentially tridentate (O,O,O) 1,1,1-tris(hydroxymethyl)ethane ($thmeH_3$, Scheme 1) group. Previous reports of Mn-containing products from reactions with $thmeH_3$ and N_3^- have included an additional *N,N*-chelate, 2,2′-bipyridine (bpy), leading to the structurally interesting complex $\left[Mn^{II}_{24}Mn^{IV}_8(thme)_{16}(bpy)_{24}(N_3)_{12}(O_2CMe)_{12}\right]^{8+}$ [42]. In the present paper, we report new high-nuclearity, mixed-valence $Mn_6^{II/III}$ molecules with $RCO_2^-/N_3^-/thme^{3-}$ ligation and an octahedral metal topology surrounded by $\{Na_4\}$ tetrahedra to yield an overall $\{Mn_6Na_4\}_n$ 3-D structure. The syntheses, structures and magnetochemical characterization of these compounds are described in this paper. In addition, we also describe the fascinating supramolecular architectures that these clusters display.

Experimental

General Data

All manipulations were performed under aerobic conditions using materials (reagent grade) and solvents as received. Infrared spectra were recorded in the solid state (KBr pellets) on a Nicolet Nexus 670 FTIR spectrometer in the 450–4000 cm^{-1} range. Elemental analyses (C, H, and N) were performed on a Perkin–Elmer 2400 Series II Analyzer. Variable-temperature direct current (dc) and alternating current (ac) magnetic susceptibility data were collected at the University of Florida using a Quantum Design MPMS-XL SQUID susceptometer equipped with a 7 T magnet and operating in the 1.8–300 K range. Samples were embedded in solid eicosane to prevent torquing. Ac magnetic susceptibility measurements were performed in an oscillating ac field of 3.5 G and a zero dc field; the oscillation frequencies were in the 50–1000 Hz range. Pascal's constants were used to estimate the diamagnetic corrections, which were subtracted from the experimental susceptibilities to give the molar paramagnetic susceptibilities (χ_M).

Synthesis of $[Mn_6Na_4O(N_3)(O_2CMe)_5(thme)_4(H_2O)_4]\cdot 4py$ (**1**·4py)

Solid $MnCl_2\cdot 4H_2O$ (0.20 g, 1.0 mmol), $NaO_2CMe\cdot 3H_2O$ (0.27 g, 2.0 mmol), and NaN_3 (0.070 g, 1.0 mmol) were added to a stirred, colorless solution of $thmeH_3$ (0.12 g, 1.0 mmol) and NEt_3 (0.14 mL, 1.0 mmol) in MeOH/pyridine (30 mL, 5:1 v/v). The resulting orange solution was stirred for 2 h, during which time all the solids dissolved and the color of the solution changed to dark red. The solution was filtered, and the filtrate left undisturbed to concentrate slowly by evaporation. After 4 days, X-ray quality dark-red crystals of **1**·4py had appeared and were collected by filtration, washed with cold MeOH (2 × 3 mL) and Et_2O (2 × 5 mL), and dried under vacuum; the yield was 45%. Anal. Calcd for **1**·4py: C, 36.80; H, 4.88; N, 6.01%. Found: C, 37.12; H, 4.92; N, 5.94%. Selected IR data (cm^{-1}): 3442 (mb), 2966 (w), 2850 (m), 2090 (s), 1659 (vs), 1596 (w), 1563 (vs), 1518 (m), 1470 (m), 1456 (m), 1433 (s), 1400 (m), 1337 (m), 1265 (m), 1200 (w), 1066 (m), 1032 (m), 999 (m), 912 (w), 888 (m), 760 (m), 735 (w), 670 (w), 644 (w), 616 (mb), 580 (m), 442 (w).

Synthesis of $[Mn_6Na_4O(N_3)(O_2CEt)_5(thme)_4(H_2O)_4]\cdot 2MeOH$ (**2**·2MeOH)

This complex was prepared in the same manner as complex **1** but using NaO_2CEt (0.19 g, 2.0 mmol) in place of $NaO_2CMe\cdot 3H_2O$. After 5 days, dark-red crystals of **2**·2MeOH were isolated, collected by filtration, washed with cold MeOH (2 × 3 mL) and Et_2O (2 × 5 mL), and dried under vacuum; the yield was 30%. Anal. Calcd for **2** (solvent-free): C, 30.34; H, 5.02; N, 3.03%. Found: C, 30.23; H, 4.87; N, 3.26%. Selected IR data (cm^{-1}): 3422 (mb), 2969 (w), 2853 (m), 2095 (s), 1669 (vs), 1596 (w), 1567 (vs), 1520 (m), 1470 (m), 1457 (m), 1430 (s), 1404 (m), 1345 (m), 1265 (m), 1201 (w), 1069 (m), 1030 (m), 1003 (m), 910 (w), 889 (m), 762 (m), 731 (w), 670 (w), 649 (w), 615 (mb), 583 (m), 440 (w).

Safety note: Azide salts are potentially explosive; such compounds should be synthesized and used in small quantities, and treated with utmost care at all times.

Crystallographic Analysis

Data were collected on a Siemens SMART PLATFORM equipped with a CCD area detector and a graphite monochromator utilizing Mo-Kα radiation ($\lambda = 0.71073$ Å). Suitable crystals of **1**·4py and **2**·2MeOH were attached to glass fibers using silicone grease and transferred to a goniostat where they were cooled to 173 K for data collection. An initial search of reciprocal space revealed a triclinic cell for **1**·4py and a monoclinic cell for **2**·2MeOH; space groups $P\bar{1}$ (**1**·4py) and $P2_1/c$ (**2**·2MeOH) were confirmed by the subsequent solution and refinement of the structures. Cell parameters were refined using up to 8192 reflections. A full sphere of data (1850 frames) was collected using the ω-scan method (0.3° framewidth). The first 50 frames were re-measured at the end of data collection to monitor instrument and crystal stability (maximum correction on I was <1%). Absorption corrections by integration were applied based on measured indexed crystal faces. The structures were solved by direct methods in *SHELXTL6* [43], and refined on F^2 using

full-matrix least-squares. The non-H atoms were treated anisotropically, whereas the H atoms were placed in calculated, ideal positions and refined as riding on their respective C atoms.

For **1**·4py, the asymmetric unit consists of the complete Mn_6Na_4 cluster and four pyridine molecules of crystallization. The latter solvent molecules are disordered and could not be modeled properly, thus program SQUEEZE [44], a part of the PLATON package of crystallographic software, was used to calculate the solvent disorder area and remove its contribution to the overall intensity data. In the Mn_6Na_4 cluster, there are three disorders: The first is the N1 azide, where N(2–3) is disordered against N(2′–3′). Second, the C(55–56) unit of an acetate ligand, along with an adjacent methanol group, is disordered against a C(55′–56′) with a water molecule; the three oxygen atoms are common to both disordered parts. The third disorder shows an acetate ion and a water molecule flip-flopping along a line of three oxygen atoms [C(27–28)/C(27′–28′)]. A total of 1327 parameters were included in the structure refinement using 18740 reflections with $I > 2\sigma(I)$ to yield R1 and *wR*2 of 5.10 and 12.58%, respectively.

For **2**·2MeOH, the asymmetric unit consists of the complete Mn_6Na_4 cluster and two methanol molecules of crystallization. The latter solvent molecules are disordered and could not be modeled properly, thus program SQUEEZE [44] was again used to calculate the solvent disorder area and remove its contribution to the overall intensity data. In the Mn_6Na_4 cluster, there are three disorders, all including the carbon atoms of the propionate groups. The first is propionate O16/O17, where C26 is disordered against C26′; the second is propionate O18/O19, where C28/C29 are disordered against C28′/C29′; and the third is propionate O22/O23, where C35 is disordered against C35′. A total of 666 parameters were included in the structure refinement on F^2 using 7905 reflections with $I > 2\sigma(I)$ to yield R1 and wR2 of 4.87 and 12.32%, respectively.

Unit cell data and details of the structure refinements for the three complexes are collected in Table 1.

Results and Discussion

Syntheses

A number of synthetic procedures to Mn clusters are available involving the reaction of an alcohol-containing chelate with a simple Mn^{II} salt or a higher oxidation state source. With carboxylates, pyridyl alcohols (see Scheme 1) such as hmpH, 2-(hydroxyethyl)pyridine (hepH), and $pdmH_2$ have given products such as $[Mn_{10}O_4(OH)_2(O_2CMe)_8(hmp)_8]^{4+}$ [28], $[Mn_{18}O_{14}(O_2CMe)_{18}(hep)_4(hepH)_2(H_2O)_2]^{2+}$ [45], and $[Mn_4(O_2CMe)_2(pdmH)_6]^{2+}$ [46], respectively, whereas ligands such as $thmeH_3$, $teaH_3$, propane-1,3-diol, and $mdaH_2$ (see Scheme 1) have led to various rod-like [47] and loop-shaped [48–50] manganese carboxylate clusters. The present study has focused on the combination of carboxylate ligands and an alcohol-containing chelate, such as $thmeH_3$, in the co-presence of N_3^- ions as ancillary ligands. We targeted

Table 1 Crystallographic data for **1**·4py and **2**·2MeOH

Parameter	**1**	**2**
Formula[a]	$C_{81}H_{150}N_{10}O_{54}Mn_{12}Na_8$	$C_{37}H_{75}N_3O_{28}Mn_6Na_4$
Fw (g mol^{-1})[a]	2971.31	1431.60
Crystal system	Triclinic	Monoclinic
Space group	$P\bar{1}$	$P2_1/c$
a (Å)	17.1431(9)	17.132(2)
b (Å)	19.8709(10)	19.514(2)
c (Å)	20.2530(10)	19.826(2)
α (°)	84.975(1)	90
β (°)	82.758(1)	109.796(2)
γ (°)	64.888(1)	90
V (Å^3)	6192.8(5)	6236.1(13)
Z	2	4
T (K)	173(2)	173(2)
Radiation (Å)[b]	0.71073	0.71073
ρ_{calc} (g cm^{-3})	1.593	1.525
μ (mm^{-1})	1.296	1.284
Measd/independent	42221/27757	42209/14303
R_{int} reflns	0.0564	0.1031
Obsd reflns [$I > 2\sigma(I)$]	18740	7905
R_1[c,d]	0.0510	0.0487
wR_2[e]	0.1258	0.1232
GOF on F^2	0.978	0.892
$(\Delta\rho)_{max,min}$ (e Å^{-3})	0.896, −0.591	0.618, −0.664

[a]Including solvate molecules, [b]Graphite monochromator, [c]$I > 2\sigma(I)$, [d]$R_1 = \Sigma(||F_o| - |F_c||)/\Sigma|F_o|$, [e]$wR_2 = [\Sigma[w(F_o^2 - F_c^2)^2]/\Sigma[w(F_o^2)^2]]^{1/2}$, $w = 1/[\sigma^2(F_o^2) + [(ap)^2 + bp]$, where $p = [\max(F_o^2, 0) + 2F_c^2]/3$

different structural motifs and properties than those previously reported from the reaction schemes Mn/RCO_2^-/thmeH$_3$ [47] and Mn/N_3^-/thmeH$_3$/bpy [42].

A variety of reactions differing in the RCO_2^- and/or N_3^- amount, the other inorganic anions or cations present, the Mn:thmeH$_3$:NEt$_3$ ratio, and/or the solvent were explored in identifying the following successful systems. The reaction of $MnCl_2{\cdot}4H_2O$, thmeH$_3$, NEt$_3$, $NaO_2CMe{\cdot}3H_2O$ and NaN_3 (1:1:1:2:1) in MeOH/pyridine gave the 3-D coordination polymer $[Mn_6Na_4O(N_3)(O_2CMe)_5(thme)_4(H_2O)_4]$ (**1**) in good (∼45%) yields. The formation of **1** is summarized in Eq. 1.

$$6Mn^{2+} + 4thmeH_3 + 10NEt_3 + 4Na^+ + N_3^- + 5MeCO_2^- + O_2 + 3\ H_2O \rightarrow \left[Mn_6Na_4O(N_3)(O_2CMe)_5(thme)_4(H_2O)_4\right] + 10\ NHEt_3^+ \quad (1)$$

The same procedure was used with NaO_2CEt instead of $NaO_2CMe{\cdot}3H_2O$ to explore if a different product might result; we have often seen in manganese carboxylate

cluster chemistry that a completely different product will often result if the carboxylate is altered [51, 52]. We rationalize this as reflecting the likelihood of equilibria involving different species in solution, and the identity of the isolated product is thus dependent on solubilities, crystallization kinetics, and other factors that can be influenced by the carboxylate employed. In the present system, however, the use of NaO_2CEt was found by crystallography to give the isostructural compound $[Mn_6Na_4O(N_3)(O_2CEt)_5(thme)_4(H_2O)_4]$ (**2**), but in lower ($\sim$30%) yields.

The syntheses involve Mn oxidation, undoubtedly by O_2 under the prevailing basic conditions, and Eq. 1 has been balanced accordingly. The NEt_3 is essential to ensure basic conditions and to act as a proton acceptor to facilitate the deprotonation of the $thmeH_3$ groups. A similar role could also be performed by the RCO_2^- ions, but in the absence of NEt_3, longer reaction times (>24 h) are required to get a significant dark red coloration, and the yields of isolated **1** and **2** are much lower (<10%). On the other hand, >2–3 equiv of NEt_3 gave oily products suggestive of mixtures that we have not been able to characterize, or insoluble amorphous precipitates that were probably Mn oxides or oxo/hydroxides. An increase in the amount of $thmeH_3$ led to pale yellow solutions indicative of Mn^{II} products, likely containing mainly or exclusively the neutral $thmeH_3$ form of the ligand. Finally, the mixed MeOH/py reaction solvent was identified as the one giving the highest product yield and purity, as well as the best quality single crystals.

Description of Structures

Complex **1**·4py crystallizes in triclinic space group $P\bar{1}$ with the $[Mn_6Na_4O(N_3)(O_2CMe)_5(thme)_4(H_2O)_4]$ molecule in a general position. The partially labeled structure is shown in Fig. 1, and selected interatomic distances and angles are listed in Table 2. The structure comprises a Mn_6 octahedral core with a central μ_6-O^{2-} ion (atom O(1)) within a Na_4 tetrahedron (Fig. 2). The Mn_6 unit is held together by twelve monoatomically-bridged O atoms of two η^2:η^3:η^3:μ_5 and two η^3:η^3:η^3:μ_6 bridging $thme^{3-}$ groups (Scheme 2). Ten of these O atoms also provide linkages between the central Mn_6 unit and the outer Na_4 tetrahedron, thus becoming μ_3. Complex **1** therefore contains an overall $[Mn_6Na_4(\mu_6\text{-}O)(\mu_3\text{-}OR)_{10}(\mu\text{-}OR)_2]^{6+}$ core (Fig. 3), with peripheral ligation provided by four η^1:η^1:μ and one η^1:η^2:μ_3 $MeCO_2^-$, one terminal (η^1) N_3^- bound to Mn(1), and four terminal H_2O molecules, one at each Na atom.

The Mn atoms are all six-coordinate with near-octahedral geometry. The oxidation states are obvious from charge considerations, the metric parameters, bond valence sum (BVS) [53, 54] calculations (Table 3), and the Jahn–Teller (JT) distortions expected for high-spin Mn^{III} ions; the Mn_6 octahedral unit of **1** (and **2**, vide infra) is thus mixed-valent $2Mn^{II}$, $4Mn^{III}$ and they are color-coded accordingly in Fig. 1. The protonation levels of the bound $thme^{3-}$ O atoms and H_2O molecules were confirmed by O BVS calculations (Table 3) to be as indicated. The Mn^{III} JT elongation axes are O(1)–Mn(1)–N(1), O(1)–Mn(2)–O(14), O(1)–Mn(3)–O(16), and O(1)–Mn(4)–O(18), each involving the central μ_6-O^{2-} ion and one of the O atoms of the $MeCO_2^-$ ligands or the bound N atom of the N_3^- group.

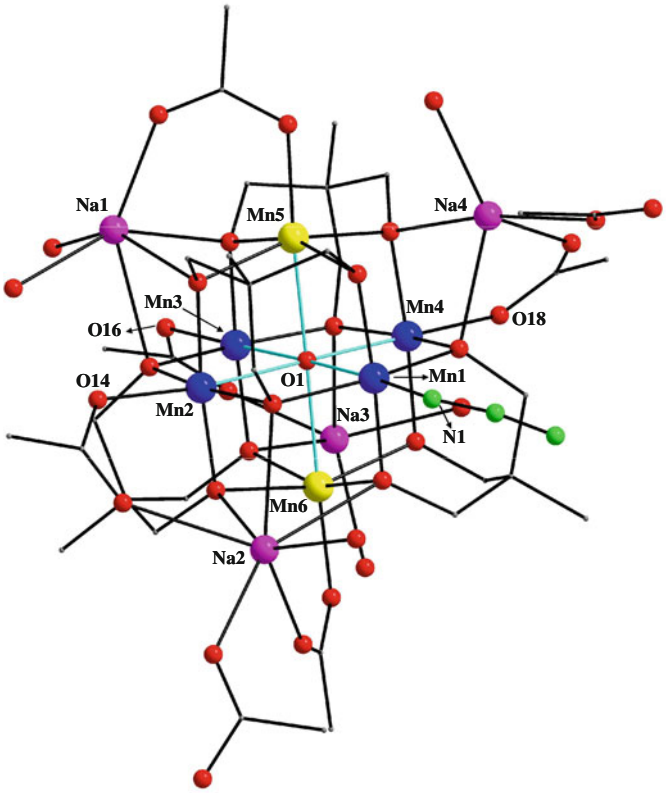

Fig. 1 Labeled PovRay representation of complex **1**, emphasizing the central $[Mn_6(\mu_6\text{-}O)]^{14+}$ octahedral core. H atoms have been omitted for clarity. Color scheme: Mn^{II} yellow; Mn^{III} blue; Na^{I} purple; O red; N green; C grey

The four Na^+ atoms in **1** are linked to those of neighboring clusters (Fig. 4, top) by two of the four terminal H_2O molecules [O(47) and O(49)] becoming μ-bridging, and two μ_2-$MeCO_2^-$ ions [O(15) and O(19)] becoming μ_3-bridging. Na atoms Na(1,3,4) are six-coordinate with distorted octahedral geometry, whereas Na(2) is seven-coordinate with distorted pentagonal bipyramidal geometry. This gives a 3-D supramolecular assembly (Fig. 4, middle and bottom) containing large channels with dimensions of approximately 7 × 10 Å.

A partially labeled representation of complex **2** is shown in Fig. 5. The molecular and supramolecular assembly of **2** is essentially the same as those of **1**, the only difference being the bulk of the carboxylate group, which causes some minor changes to the separations between neighboring $\{Mn_6Na_4\}$ units and an expected small decrease in the size of the channels through the structure. Otherwise the two structures are very similar, and the structure of **2** will thus not be further discussed.

There have been a large number of Mn_6 complexes reported in the literature, and these possess a wide variety of metal topologies such as fused triangles, rods, wheels, and so forth, as well as different oxidation state levels. Complexes **1** and **2**

Table 2 Selected interatomic distances (Å) and angles (°) for complex **1**·4py[a]

Mn(1)···Mn(2)	3.170(7)	Mn(2)···Mn(6)	3.177(7)
Mn(1)···Mn(3)	4.500(7)	Mn(3)···Mn(4)	3.133(7)
Mn(1)···Mn(4)	3.177(7)	Mn(3)···Mn(5)	3.208(8)
Mn(1)···Mn(5)	3.187(8)	Mn(3)···Mn(6)	3.217(7)
Mn(1)···Mn(6)	3.206(7)	Mn(4)···Mn(5)	3.159(7)
Mn(2)···Mn(3)	3.141(7)	Mn(4)···Mn(6)	3.180(7)
Mn(2)···Mn(4)	4.425(7)	Mn(5)···Mn(6)	4.565(7)
Mn(2)···Mn(5)	3.198(7)	Mn(6)–O(1)	2.300(2)
Mn(1)–O(1)	2.268(3)	Mn(6)–O(3)	2.148(2)
Mn(1)–O(2)	1.998(3)	Mn(6)–O(4)	2.125(3)
Mn(1)–O(4)	1.911(2)	Mn(6)–O(11)	2.137(2)
Mn(1)–O(5)	1.914(2)	Mn(6)–O(12)	2.168(2)
Mn(1)–O(6)	2.022(2)	Mn(6)–O(22)	2.101(2)
Mn(1)–N(1)	2.137(4)	Na(1)–O(7)	2.422(3)
Mn(2)–O(1)	2.267(3)	Na(1)–O(9)	2.400(3)
Mn(2)–O(6)	2.001(2)	Na(1)–O(13)	2.573(3)
Mn(2)–O(7)	1.925(2)	Na(1)–O(21)	2.323(3)
Mn(2)–O(11)	1.915(2)	Na(1)–O(47)	2.368(3)
Mn(2)–O(13)	2.015(2)	Na(1)–O(47′)	2.384(3)
Mn(2)–O(14)	2.093(2)	Na(2)–O(4)	2.764(3)
Mn(3)–O(1)	2.233(3)	Na(2)–O(6)	2.594(3)
Mn(3)–O(9)	1.911(2)	Na(2)–O(11)	2.408(3)
Mn(3)–O(10)	1.999(2)	Na(2)–O(15)	2.744(3)
Mn(3)–O(12)	1.925(2)	Na(2)–O(23)	2.546(3)
Mn(3)–O(13)	2.002(2)	Na(2)–O(46″)	2.397(3)
Mn(3)–O(16)	2.112(3)	Na(2)–O(48)	2.368(4)
Mn(4)–O(1)	2.159(3)	Na(3)–O(3)	2.884(3)
Mn(4)–O(2)	2.069(3)	Na(3)–O(10)	2.353(3)
Mn(4)–O(3)	1.913(2)	Na(3)–O(12)	2.381(3)
Mn(4)–O(8)	1.931(2)	Na(3)–O(17)	2.361(3)
Mn(4)–O(10)	2.072(3)	Na(3)–O(49)	2.362(3)
Mn(4)–O(18)	2.078(3)	Na(3)–O(49$^{\#}$)	2.386(3)
Mn(5)–O(1)	2.266(2)	Na(4)–O(2)	2.427(3)
Mn(5)–O(5)	2.157(3)	Na(4)–O(5)	2.944(3)
Mn(5)–O(7)	2.136(2)	Na(4)–O(8)	2.330(3)
Mn(5)–O(8)	2.143(2)	Na(4)–O(19)	2.416(3)
Mn(5)–O(9)	2.176(2)	Na(4)–O(44)	2.247(3)
Mn(5)–O(20)	2.080(3)	Na(4)–O(50)	2.350(4)
Mn(1)–O(1)–Mn(2)	88.7(9)	Mn(2)–O(11)–Mn(6)	103.2(1)
Mn(1)–O(1)–Mn(3)	177.3(1)	Mn(2)–O(13)–Mn(3)	102.9(1)
Mn(1)–O(1)–Mn(4)	91.7(1)	Mn(3)–O(1)–Mn(4)	91.0(1)
Mn(1)–O(1)–Mn(5)	89.3(9)	Mn(3)–O(1)–Mn(5)	90.9(9)
Mn(1)–O(1)–Mn(6)	89.1(9)	Mn(3)–O(1)–Mn(6)	90.4(9)

Table 2 continued

Mn(1)–O(2)–Mn(4)	102.7(1)	Mn(3)–O(9)–Mn(5)	103.2(1)
Mn(1)–O(4)–Mn(6)	105.0(1)	Mn(3)–O(10)–Mn(4)	100.6(1)
Mn(1)–O(5)–Mn(5)	102.9(1)	Mn(3)–O(12)–Mn(6)	103.5(1)
Mn(1)–O(6)–Mn(2)	104.0(1)	Mn(4)–O(1)–Mn(5)	91.1(9)
Mn(2)–O(1)–Mn(3)	88.5(9)	Mn(4)–O(1)–Mn(6)	90.9(9)
Mn(2)–O(1)–Mn(4)	179.0(1)	Mn(4)–O(3)–Mn(6)	103.0(1)
Mn(2)–O(1)–Mn(5)	89.7(9)	Mn(4)–O(8)–Mn(5)	101.6(1)
Mn(2)–O(1)–Mn(6)	88.1(9)	Mn(5)–O(1)–Mn(6)	177.5(1)
Mn(2)–O(7)–Mn(5)	103.8(1)		

[a] Unprimed, primed, double-primed, and #-labeled atoms are related by symmetry

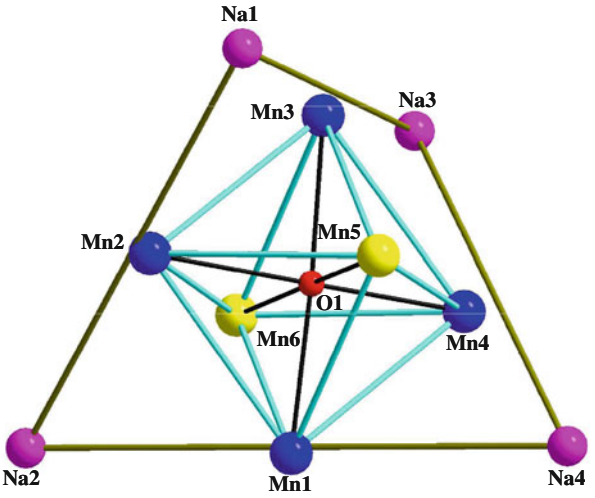

Fig. 2 The Mn_6Na_4 topology of **1**, emphasizing the $[Mn_6(\mu_6\text{-}O)]^{14+}$ octahedron and Na_4 tetrahedron. Dark cyan and orange lines indicate the Mn…Mn and Na…Na vectors, respectively. Color scheme as in Fig. 1

Scheme 2 The coordination modes of $thme^{3-}$ found in complexes **1** and **2**

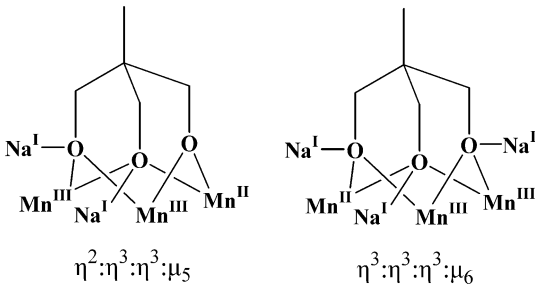

are rare examples of hexanuclear molecular species with an $[M_6(\mu_6\text{-}O^{2-})]$ octahedral core [55–61], only the second and third in Mn coordination chemistry [62], and the first at the $2Mn^{II}$, $4Mn^{III}$ oxidation level. Further, **1** and **2** are the first

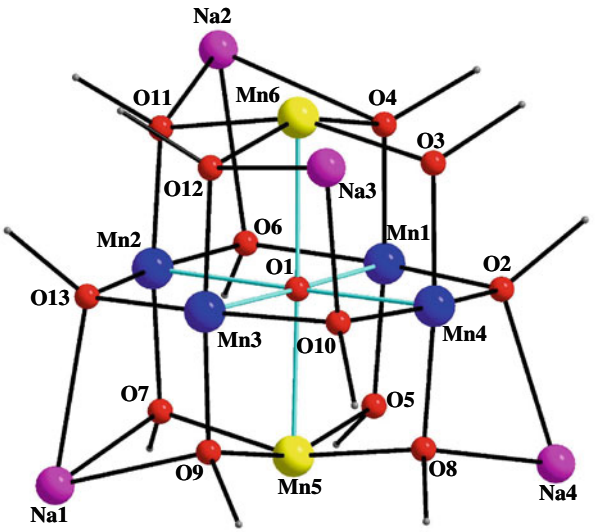

Fig. 3 Labeled PovRay representation of the complete $[Mn_6Na_4(\mu_6\text{-}O)(\mu_3\text{-}OR)_{10}(\mu\text{-}OR)_2]^{6+}$ core of **1**, emphasizing the central $[Mn_6(\mu_6\text{-}O)]^{14+}$ unit. Color scheme as in Fig. 1

Table 3 BVS calculations[a,b] for Mn, Na, and selected O atoms in **1**

Atom	Mn^{II}	Mn^{III}	Mn^{IV}
Mn1	3.09	2.85	2.95
Mn2	3.02	2.77	2.90
Mn3	3.06	2.79	2.93
Mn4	2.96	2.71	2.84
Mn5	2.09	1.91	2.01
Mn6	2.07	1.90	1.99
	Mn^{II}	Na^{I}	
Na1	1.07	1.18	
Na2	0.92	1.02	
Na3	1.03	1.14	
Na4	1.08	1.19	

	BVS	Assignment	Group
O1	1.70	O^{2-} (μ_6)	
O3	1.75	RO^{-} (μ)	$thme^{3-}$
O5	1.78	RO^{-} (μ)	$thme^{3-}$
O47	0.43	H_2O (μ)	
O49	0.43	H_2O (μ)	

[a] The underlined value is the one closest to the charge for which it was calculated. The oxidation state is the nearest whole number to the underlined value

[b] An O BVS in the ~1.7–2.0, ~1.0–1.2, and ~0.2–0.4 ranges is indicative of non-, single- and double-protonation, respectively

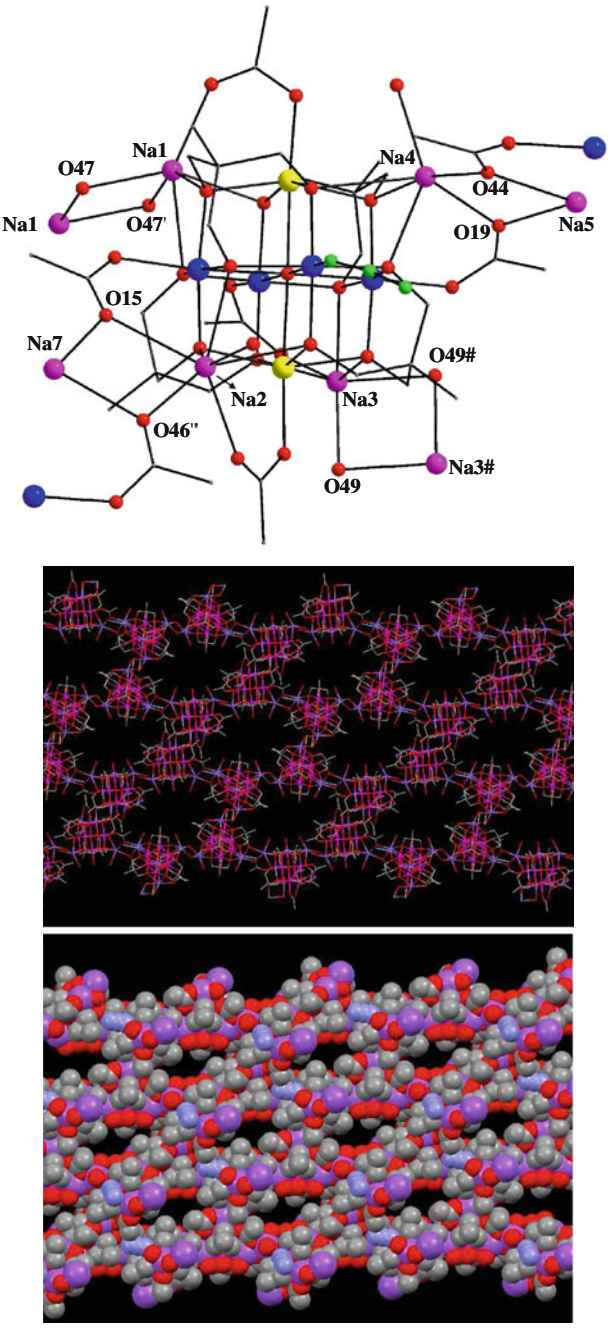

Fig. 4 The polymeric structure of **1**. (top) View showing the connectivity of the Mn_6Na_4 units. (middle) Wire-frame and (bottom) space-filling representations viewed along the *c* axis, emphasizing the large channels. H atoms have been omitted for clarity. Color scheme: Mn pink; Na purple; O red; N light blue; C grey

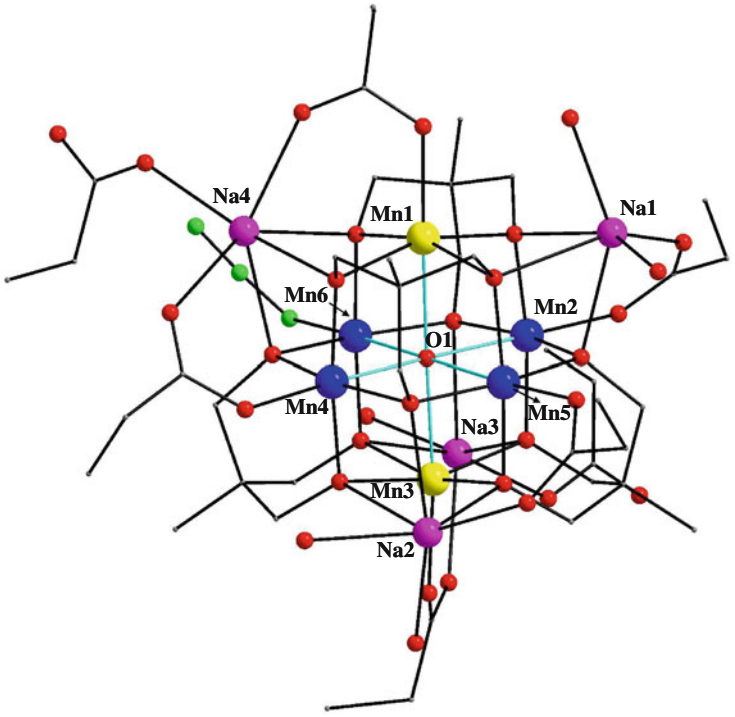

Fig. 5 Labeled PovRay representation of complex **2**, emphasizing the central $[Mn_6(\mu_6\text{-}O)]^{14+}$ octahedral core. H atoms have been omitted for clarity. Color scheme as in Fig. 1

Mn_6 clusters connected to four Na^I atoms, thereby giving a 3-D supramolecular motif.

Magnetochemistry

Dc and ac magnetic susceptibility studies of ***1***. Variable-temperature, solid-state magnetic susceptibility measurements were performed on powdered polycrystalline samples of **1**·4py and **2**, restrained in eicosane to prevent torquing, in a 1 kG (0.1 T) field and in the 5.0–300 K range. The obtained magnetic data for **1**·4py and **2** are essentially superimposable, and thus only those of the former are shown as a $\chi_M T$ versus T plot in Fig. 6. $\chi_M T$ for **1**·4py rapidly decreases from 16.55 cm^3Kmol^{-1} at 300 K to 2.47 cm^3Kmol^{-1} at 5.0 K. The 300 K value is much less than the spin-only ($g = 2$) value of 20.75 cm^3Kmol^{-1} for two Mn^{II} and four Mn^{III} non-interacting ions, indicating the presence of dominant intramolecular antiferromagnetic exchange interactions. The 5.0 K data appear to be heading for zero at 0 K, suggesting an $S = 0$ ground state spin for **1**. Given the large size and low symmetry of the Mn_6 magnetic unit within **1**, and thus the resulting number of inequivalent exchange constants, it is not possible to apply the Kambe method [63] to determine the individual pairwise Mn_2 exchange interaction parameters.

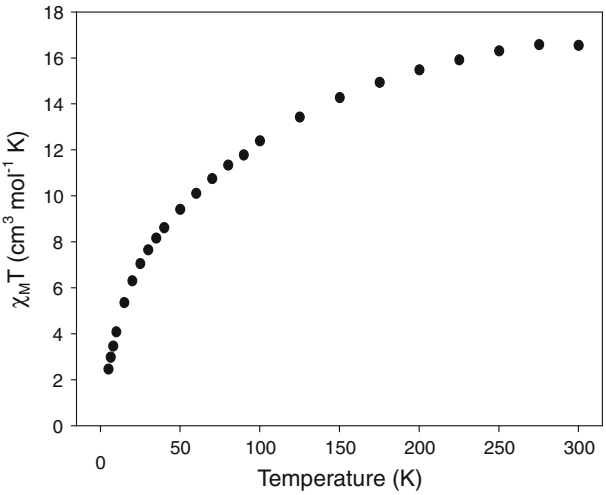

Fig. 6 $\chi_M T$ versus T plot for complex **1**·4py in a 1 kG dc field

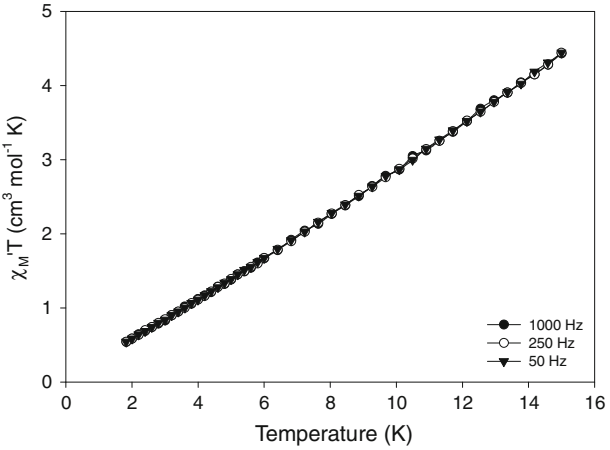

Fig. 7 Plot of the ac in-phase $\chi'_M T$ versus T for complex **1**·4py at the indicated frequencies

As we have described before on many occasions, ac susceptibility studies are a powerful complement to dc studies for determining the ground state of a system, because they preclude any complications arising from the presence of a dc field. Ac studies also allow the slow magnetization relaxation of a SMM to be detected, since this would give a non-zero out-of-phase (χ''_M) susceptibility signal due to the compound's magnetization vector not being able to keep up with the oscillating field. We thus carried out ac studies on complex **1**·4py in the 1.8–15 K range using a 3.5 G ac field oscillating at frequencies in the 50–1000 Hz range. The in-phase $\chi'_M T$ signal (analogous to the dc $\chi_M T$) shows a steep decrease below 15 K (Fig. 7) and is

clearly heading for $\chi'_M T = 0$ at 0 K, thus confirming an $S = 0$ ground state. Consequently, there is no possibility of an out-of-phase signal, and none was seen (not shown). The decrease in $\chi'_M T$ below 15 K is due to depopulation of excited states as the temperature is lowered, and the steepness of the decrease in this narrow temperature range is a clear indication of a high density of low-lying excited states, as indeed is expected for a molecule containing multiple Mn^{II} atoms, since these are known to give very weak exchange interactions. It should be added that although the structure of **1**·4py is a 3-D network, magnetically it is expected to behave as a collection of essentially non-interacting $\{Mn_6Na_4\}$ molecules, because the long superexchange interaction pathways via the linking diamagnetic Na atoms will result in at best only extremely weak intermolecular interactions.

Summary and Conclusions

The combination of azide, carboxylate and thmeH_3 ligands in Mn cluster chemistry has yielded a new family of decanuclear heterometallic Mn_6Na_4 complexes with an unprecedented 'octahedron-within-tetrahedron' topology and an aesthetically pleasing 3-D supramolecular motif. These 3-D networks were prepared under mild room temperature conditions with self-assembly processes directed by metal–ligand coordination, and have open-framework structures with nanometer-sized channels. The mixed-valence $Mn^{II}_2Mn^{III}_4$ magnetic units within the polymeric structures of **1** and **2** are antiferromagnetically-coupled with $S = 0$ ground states. The network architectures of **1**·4py and **2**·2MeOH and the nanoporous channels they contain offer the possibility for interesting study of gas absorption into these channels and/or diffusion of gas through them, as we recently reported for the diffusion of Xe gas through the nanopores of crystals of Ga_{10} and Ga_{18} molecular wheels [64].

Supplementary Information

Crystallographic data in CIF format have been deposited at the Cambridge Crystallographic Data Centre with CCDC Nos. 769069 (**1**·4py) and 769070 (**2**·2MeOH). Copies of this information may be obtained free of charge from The Director, CCDC, 12 Union Road, Cambridge, CB2 1EZ, UK (Fax: +44-1223-336033; e-mail: deposit@ccdc.cam.ac.uk or http://www.ccdc.cam.ac.uk).

Acknowledgements We thank the U.S. National Science Foundation (Grant CHE-0910472) for support of this work.

References

1. R. E. P. Winpenny, in J. A. McCleverty and T. J. Meyer (eds.), *Comprehensive Coordination Chemistry II*, vol.7 (Elsevier, Amsterdam, 2004), pp. 125–175).
2. V. L. Pecoraro (ed.), *Manganese Redox Enzymes* (VCH Publishers, New York, 1992).
3. J. Barber and J. W. Murray (2008). *Coord. Chem. Rev.* **252**, 233.

4. K. N. Ferreira, T. M. Iverson, K. Maghlaoui, J. Barber, and S. Iwata (2004). *Science* **303**, 1831.
5. C. S. Mullins and V. L. Pecoraro (2008). *Coord. Chem. Rev.* **252**, 416.
6. I. J. Hewitt, J. K. Tang, N. T. Maddhu, R. Clérac, G. Buth, C. F. Anson, and A. K. Powell (2006). *Chem. Commun.* 2650.
7. A. Mishra, W. Wernsdorfer, K. A. Abboud, and G. Christou (2005). *Chem. Commun*. 54.
8. A. M. Ako, I. J. Hewitt, V. Mereacre, R. Clérac, W. Wernsdorfer, C. E. Anson, and A. K. Powell (2006). *Angew. Chem. Int. Ed.* **45**, 4926.
9. C.-H. Ge, Z.-H. Ni, C.-M. Liu, A.-L. Cui, D.-Q. Zhang, and H.-Z. Kou (2008). *Inorg. Chem. Commun.* **11**, 675.
10. E. E. Moushi, Th. C. Stamatatos, W. Wernsdorfer, V. Nastopoulos, G. Christou, and A. J. Tasiopoulos (2009). *Inorg. Chem.* **48**, 5049.
11. S. Nayak, L. M. C. Beltran, Y. Lan, R. Clérac, N. G. R. Hearns, W. Wernsdorfer, C. E. Anson, and A. K. Powell (2009), *Dalton Trans.*1901.
12. Th. C. Stamatatos, K. A. Abboud, W. Wernsdorfer, and G. Christou (2007). *Angew. Chem. Int. Ed.* **46**, 884.
13. O. Kahn *Molecular Magnetism* (VCH Publishers, New York, 1993).
14. Th. C. Stamatatos and G. Christou (2008). *Phil. Trans. R. Soc. A* **366**, 113.
15. M. Murrie and D. J. Price (2007). *Annu. Rep. Prog. Chem., Sect. A* **103**, 20.
16. G. Aromi and E. K. Brechin (2006). *Struct. Bond.* **122**, 1.
17. R. Birchner, G. Chaboussant, C. Dobe, H. Güdel, S. T. Ochsenbein, A. Sieber, and O. Waldman (2006). *Adv. Funct. Mater.* **16**, 209.
18. D. Gatteschi and R. Sessoli (2003). *Angew. Chem. Int. Ed.* **42**, 268.
19. J. R. Long in P. Yang (ed.), *Chemistry of Nanostructured Materials* (World Scientific Publishing, Hong Kong, 2003), p. 291.
20. G. Christou, D. Gatteschi, D. N. Hendrickson, and R. Sessoli (2000). *MRS Bull.* **25**, 66.
21. G. Christou (2005). *Polyhedron* **24**, 2065. and references therein.
22. R. Bagai and G. Christou (2009). *Chem. Soc. Rev.* **38**, 1011. and references therein.
23. Th. C. Stamatatos and G. Christou (2009). *Inorg. Chem.* **48**, 3308.
24. A. J. Tasiopoulos, A. Vinslava, W. Wernsdorfer, K. A. Abboud, and G. Christou (2004). *Angew. Chem. Int. Ed.* **43**, 2117.
25. Th. C. Stamatatos, K. A. Abboud, W. Wernsdorfer, and G. Christou (2006). *Angew. Chem. Int. Ed.* **45**, 4134.
26. Th. C. Stamatatos, K. A. Abboud, W. Wernsdorfer, and G. Christou (2007). *Polyhedron* **26**, 2042.
27. Th. C. Stamatatos, K. M. Poole, K. A. Abboud, W. Wernsdorfer, T. A. O'Brien, and G. Christou (2008). *Inorg. Chem.* **47**, 5006.
28. N. C. Harden, M. A. Bolcar, W. Wernsdorfer, K. A. Abboud, W. E. Streib, and G. Christou (2003). *Inorg. Chem.* **42**, 7067.
29. C. Boskovic, E. K. Brechin, W. E. Streib, K. Folting, J. C. Bollinger, D. N. Hendrickson, and G. Christou (2002). *J. Am. Chem. Soc.* **124**, 3725.
30. M. Murugesu, M. Habrych, W. Wernsdorfer, K. A. Abboud, and G. Christou (2004). *J. Am. Chem. Soc.* **126**, 4766.
31. E. K. Brechin, J. Yoo, J. C. Huffman, D. N. Hendrickson, and G. Christou (1999). *Chem. Commun.* 783.
32. C. Boskovic, W. Wernsdorfer, K. Folting, J. C. Huffman, D. N. Hendrickson, and G. Christou (2002). *Inorg. Chem.* **41**, 5107.
33. M. Murugesu, W. Wernsdorfer, K. A. Abboud, and G. Christou (2005). *Angew. Chem. Int. Ed.* **44**, 892.
34. Th. C. Stamatatos, K. M. Poole, D. Foguet-Albiol, K. A. Abboud, T. A. O'Brien, and G. Christou (2008). *Inorg. Chem.* **47**, 6593.
35. D. Foguet-Albiol, T. A. O'Brien, W. Wernsdorfer, B. Moulton, M. J. Zaworotko, K. A. Abboud, and G. Christou (2005). *Angew. Chem. Int. Ed.* **44**, 897.
36. Th. C. Stamatatos, D. Foguet-Albiol, K. M. Poole, W. Wernsdorfer, K. A. Abboud, T. A. O'Brien, and G. Christou (2009). *Inorg. Chem.* **48**, 9831.
37. C. C. Stoumpos, I. A. Gass, C. J. Milios, N. Lalioti, A. Terzis, G. Aromi, S. J. Teat, E. K. Brechin, and S. P. Perlepes (2009). *Dalton Trans.* 307.
38. Th. C. Stamatatos, K. A. Abboud, W. Wernsdorfer, and G. Christou (2008). *Angew. Chem. Int. Ed.* **47**, 6694.

39. C. J. Milios, E. Kefalloniti, C. P. Raptopoulou, A. Terzis, R. Vicente, N. Lalioti, A. Escuer, and S.P. Perlepes (2003). *Chem. Commun.* 819.
40. A. Escuer and G. Aromi (2006). *Eur. J. Inorg. Chem.* **23**, 4721.
41. E. Ruiz, J. Cano, S. Alvarez, and P. Alemany (1998). *J. Am. Chem. Soc.* **120**, 11122.
42. R. T. W. Scott, S. Parsons, M. Murugesu, W. Wernsdorfer, G. Christou, and E. K. Brechin (2005). *Angew. Chem. Int. Ed.* **45**, 6540.
43. *SHELXTL6*; Bruker-AXS, Madison, WI, 2000.
44. P. Van der Sluis and A. L. Spek (1990). *Acta Crystallogr., Sect. A: Found Crystallogr.* **A46**, 194.
45. E. K. Brechin, E. C. Sanudo, W. Wernsdorfer, C. Boskovic, J. Yoo, D. N. Hendrickson, A. Yamaguchi, H. Ishimoto, T. E. Concolino, A. L. Rheingold, and G. Christou (2005). *Inorg. Chem.* **44**, 502.
46. J. Yoo, E. K. Brechin, A. Yamaguchi, M. Nakano, J. C. Huffman, A. L. Maniero, L.-C. Brunel, K. Awaga, H. Ishimoto, G. Christou, and D. N. Hendrickson (2000). *Inorg. Chem.* **39**, 3615.
47. G. Rajaraman, M. Murugesu, E. C. Sanudo, M. Soler, W. Wernsdorfer, M. Helliwell, C. Muryn, J. Raftery, S. J. Teat, G. Christou, and E. K. Brechin (2004). *J. Am. Chem. Soc.* **126**, 15445.
48. E. E. Moushi, Th. C. Stamatatos, W. Wernsdorfer, V. Nastopoulos, G. Christou, and A. J. Tasiopoulos (2006). *Angew. Chem. Int. Ed.* **45**, 7722.
49. E. E. Moushi, C. Lampropoulos, W. Wernsdorfer, V. Nastopoulos, G. Christou, and A. J. Tasiopoulos (2007). *Inorg. Chem.* **46**, 3795.
50. S. J. Shah, C. M. Ramsey, K. J. Heroux, A. G. DiPasquale, N. S. Dalal, A. L. Rheingold, E. del Barco, and D. N. Hendrickson (2008). *Inorg. Chem.* **47**, 9569.
51. P. King, W. Wernsdorfer, K. A. Abboud, and G. Christou (2005). *Inorg. Chem.* **44**, 8659.
52. T. Taguchi, M. R. Daniels, K. A. Abboud, and G. Christou (2009). *Inorg. Chem.* **48**, 9325.
53. I. D. Brown and D. Altermatt (1985). *Acta Crystallogr.* **41**, 244.
54. W. Liu and H. H. Thorp (1993). *Inorg. Chem.* **32**, 4102.
55. Y.-B. Jiang, H.-Z. Kou, R.-J. Wang, A.-L. Cui, and J. Ribas (2005). *Inorg. Chem.* **44**, 709.
56. M. I. Khan, Q. Chen, H. Hope, S. Parkin, C. J. O'Connor, and J. Zubieta (1993). *Inorg. Chem.* **32**, 2929.
57. K. Hegetschweiler, H. Schmalle, H. M. Streit, and W. Schneider (1990). *Inorg. Chem.* **29**, 3625.
58. M. I. Khan, Q. Chen, J. Zubieta, and D. P. Goshom (1992). *Inorg. Chem.* **31**, 1556.
59. K. Hegetschweiler, H. Schmalle, H. M. Streit, V. Gramlich, and H.-U. Hund (1992). *Inorg. Chem.* **31**, 1299.
60. A. Cornia, D. Gatteschi, K. Hegetschweiler, L. Hausherr-Primo, and V. Gramlich (1996). *Inorg. Chem.* **35**, 4414.
61. J. Spandl, M. Kusserow, and I. Brudgam (2003). *Z Anorg. Allg. Chem.* **629**, 968.
62. Th. C. Stamatatos, K. V. Pringouri, K. A. Abboud, and G. Christou (2009). *Polyhedron* **28**, 1624.
63. K. Kambe (1950). *J. Phys. Soc. Jpn.* **5**, 48.
64. C.-Y. Cheng, Th. C. Stamatatos, G. Christou, and C. R. Bowers (2010). *J. Am. Chem. Soc.* **132**, 5387.